Electrochimica Acta 169 (2015) 395–401

Contents lists available at ScienceDirect

Electrochimica Acta

journal homepage: www.elsevier.com/locate/electacta

Enhanced dye loading-light harvesting TiO_2 photoanode with screen printed nanorod-nanoparticles assembly for highly efficient solar cell

Mahsa Jalali [a,b], Roozbeh Siavash Moakhar [a,b], Ajay Kushwaha [b], Gregory Kia Liang Goh [b], Nastaran Riahi-Noori [c], Sayed Khatiboleslam Sadrnezhaad [a,*]

[a] Departments of Materials Science and Engineering, Sharif University of Technology, Azadi Avenue, PO Box 11155-9466, Tehran, Iran
[b] Institute of Materials Research and Engineering, Agency for Science, Technology and Research (A*STAR), 3 Research Link, 117602, Singapore
[c] Niroo Research Institute, Chemistry and Materials Division, Non-Metallic Materials Group, Tehran, Iran

ARTICLE INFO

Article history:
Received 3 February 2015
Received in revised form 23 March 2015
Accepted 14 April 2015
Available online 16 April 2015

Keywords:
TiO_2
nanorod-nanoparticle assembly
double layer photoanode
DSSC
dye loading

ABSTRACT

Morphology tailored TiO_2 nano assemblies consisting of nanorods with and without nanoparticle attachments were hydrothermally synthesized and their characteristics and light scattering properties were determined by x-ray diffraction (XRD), nitrogen sorption analysis, scanning electron microscopy (SEM), transmission electron microscopy (TEM), electrochemical impedance spectroscopy (EIS) and ultraviolet–visible spectroscopy (UV–Vis). The nanorod-nanoparticles (NR-NP) assemblies and smooth nanorod (NR) double layers were screen printed onto fluorine doped tin oxide coated glass underlayers to fabricate dye-sensitized solar cell (DSSC) photoanodes. The double layer heterogeneous hierarchical NR-NP decoration had wide Brunauer–Emmett–Teller (BET) area which resulted in 45.1% dye loading capacity, 18.96 mA cm^{-2} photocurrent and average photoanode efficiency of 8.07% which was 21% greater than NRs photoanode efficiency. Distinct NR-NPs morphology indicated multiple wave trapping and strong light scattering which was as high as 89.2%. Improvements in NR-NPs DSSCs performance were obtained because of lower resistance to charge transfer (10.07 Ω) and faster diffusion of electrolyte ions (1.22 Mho).

1. Introduction

Solar cells are promising energy conversion devices having inherent potential for partial fulfillment of future world energy demands [1]. Dye-sensitized solar cell has demonstrated strong capability due to its high efficiency, low production cost and negligible negative environmental effect [2–4]. A typical DSSC cell is a combined sandwich structure of: (a) semiconductor (e.g. TiO_2) photoanode, (b) counter electrode and (d) electrolyte [5–7]. In a single layer DSSC anode, titania is generally used as a base material for its high absorptivity of the photon absorbing dye [8]. Their performance is, however, impaired by poor electron transport, too many surface traps, repeated charge recombination and low light scattering capabilities.

Since transmission of light through the electrode without interaction with the dye lowers the cell efficiency [9], a new design is required to tailor the photoanode morphology for excellent light-scattering behavior [10]. As a result, hierarchical double-layer photoanodes are fabricated from different TiO_2 nanostructures to stimulate multi-angle light-scattering sways [11–14]. Greater scattering in the DSSC will prolong light beam journey through the photoanode and encourages the interaction of the incident photons with the dye molecules [15].

Two strategies have been employed in the past for fabrication of two-layer anodes [16]. Using large particles as overlayer and soft underlayer for scattering of the incident light has been one strategy. Small dye loading capability due to low surface area has been a shortcoming of this method [16]. The second strategy has consisted of one-dimensional (1D) nanostructures such as nanorods [9,17], nanowires [18,19], nanotubes [20,21], nanofibers [22] and nanospindles [23,24]. All these have been used as a scattering layer. Dye adsorption on such one-dimensional nanostructures has often been inadequate due to their relatively small surfaces.

Design and development of multifunctional materials that can help fabrication of highly efficient DSSCs has, therefore, been thought essentially desirable. Examples of techniques used for making the DSSC anodes have been Doctor blading [25], vacuum cold spraying [26], spin coating [27] and electrospinning [28]. For large-scale production, these methods have generally been infeasible. Screen printing, on the other hand, has proved precise

* Corresponding author.
E-mail address: sadrnezh@sharif.edu (S.K. Sadrnezhaad).

http://dx.doi.org/10.1016/j.electacta.2015.04.077
0013-4686/

control of the coating position and thickness, cost-effective and practicable [29,17,24,30,31].

This paper presents a novel method for production of highly efficient DSSCs having photoanodes fabricated by screen printing of 20–30 nm diameter TiO_2 nanoparticles attached to 300–500 nm long nanorods of 50 nm average diameter onto fluorine doped tin oxide coated glass under layer. The double layered heterogeneous nanorod-nanoparticle assembly acts as scattering layer. For comparison, a double layered DSSC made of smooth nanorod (NR) is also fabricated. TiO_2 nanorod-nanoparticles (NR-NP) based photoanode shows considerably higher light scattering and larger (45.1%) dye loading as compared to the smooth nanorod based anode. Largely enhanced photovoltaic performance of DSSCs having nanorod-nanoparticles photoanode is evident from cell efficiency of 8.07% and 18.96 mA cm^{-2} photocurrent. These heterogeneous structures are thus capable of improving the light management in the future solar devices and design and manufacturing of the double layered highly efficient dye-sensitized solar cells.

2. Experimental procedure

2.1. Nanomaterials synthesis

Hydrothermal synthesise of TiO_2 nanoparticles (NP) has been reported elsewhere [32]. Briefly, 12 g of acetic acid (CH_3COOH) was added to 58.6 g of titanium tetraisopropoxide (TTIP). This sol was then stirred for 30 min at room temperature and then 300 ml deionized water was added to it. After a further 1 h stirring, 10 ml of 65% nitric acid (Merck) was added to the sol. The mixture was heated up to 70 °C and peptized for 75 min. After that, it was poured into a 50 ml Teflon-lined stainless steel autoclave and placed in an oven at 180 °C for 24 h.

A two-step hydrothermal process was used to synthesize TiO_2 smooth nanorods (NR). First, 1 g of NP was used as precursor. It was mixed with 40 ml of 10 M aqueous NaOH and stirred for 1 h. The solution was transferred to autoclave and kept at 180 °C for 72 h. When the autoclave was cooled off to the room temperature, the resulting solution was rinsed with HCl until its pH reduced to 2. In the second step, the above solution was dispersed in 40 ml ethanol/water (1:1) solution and stirred for 30 min, then 2 ml of dimethylamine (DMA) was added and stirred again for 30 min. The finalized sol was transferred to the autoclave and kept at 180 °C for 10 h. Nanorods were used as precursor to grow TiO_2 nanoparticles on them. Assembled nanorods were also prepared by the same way mentioned (second step of NR production), except that ethylene glycol (5/3) was used instead of ethanol. Schematic representation of the synthesis process is given in the supplementary Scheme S1.

2.2. Characterizations

FESEM (Carl Zeiss, SIGMA FE-SEM unit) was used for morphological investigations. X-ray diffraction (XRD) and X'Pert Pro MPD (PANalytical) diffractometer equipped with Ni-filtered Cu-Kα radiation unit was used for crystal structure determination. The ultraviolet–visible spectroscopy (UV–Vis) 6705 JENWAY spectrometer was used to analyse the diffuse reflection spectrum (DRS) of the samples. The Brunauer–Emmett–Teller (BET) equation applied to nitrogen physisorption experiments using a Micromeritics Tristar 3000 analyser gave the specific surface areas of the synthesized powders. UV–vis absorption spectra were recorded by using a UV-3101PC UV–vis spectrophotometer. The dye loading on each photoanode was determined from the Uv–vis absorbance spectra of the desorbed dye into 0.1 M NaOH aqueous solution.

2.3. DSSC fabrication

For DSSC fabrication, a layer of paste made of NPs was screen printed onto fluorine doped tin oxide (FTO pre-treated with 40 mM $TiCl_4$) coated glass (15 Ω/square). After drying, a light scattering layer of NR-NP or NR was screen printed. The produced photoanode was then annealed at 450 °C under air. It was treated further with $TiCl_4$ and cured at 450 °C under air for 60 min. Photo-image of the samples are shown in Fig. S1. The photoanode was then finally immersed in 0.5 mM N719 solution in ethanol and kept away from light for 24 h at the room temperature. This photoelectrode and the Pt counter electrode were then assembled together with a 60 μm thick Surlyn polymer foil as the spacer and the electrolyte was injected into the space between them. The electrolyte solution consisted of 0.6 M 1-methyl propyl imidazolium iodide, 0.1 M lithium iodide, 0.05 M iodine and 0.5 M tert-butyl pyridine in acetonitrile (all from Merck). DSSCs fabricated utilising nanorods as the scattering layer were referred to as NR while that utilising nanoparticles-nanorod assembly were termed NP-NR, Fig. 1.

The photovoltaic characteristics of the DSSCs were measured using a solar simulator under 1.5 AM (100 mW cm^{-2}) irradiation to obtain a current density versus voltage (J–V) plot. Using a 75W Xenon arc lamp as the light source coupled to a monochromator, the incident photon-to-current conversion efficiency (IPCE) spectra of the devices were also measured. Furthermore, electrochemical impedance spectra data was collected using an Autolab PGSTAT302N equipped with FRA32 M over a frequency range of 0.05–50000 Hz under AM 1.5 light. The magnitude of the AC modulation signal was 10 mV. In order to fit the experimental data with an equivalent circuit, the Nova 1.10 software was used.

3. Results and discussion

3.1. Structural Properties

Fig. 2 shows X-ray diffraction (XRD) of the synthesized nanostructures. As can be seen, all the patterns of nanorods and nanorod-nanoparticles assemblies match well with the JCPDS file no. 21-1272 as per anatase phase of TiO_2. As can be expected, NR-NP has smaller crystallite sizes. The sharp and strong XRD peaks of the as-prepared TiO_2 attest good crystallinity and high purity of the anatase phase.

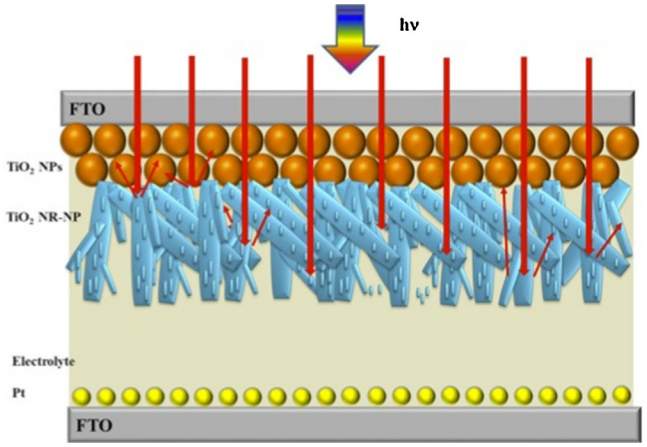

Fig. 1. Schematic illustration of NR-NP based double layer DSSC. The light scatters from NR-NP surface leading to multiple trapping and absorption within this nanostructure geometry as shown in red colour light rays.

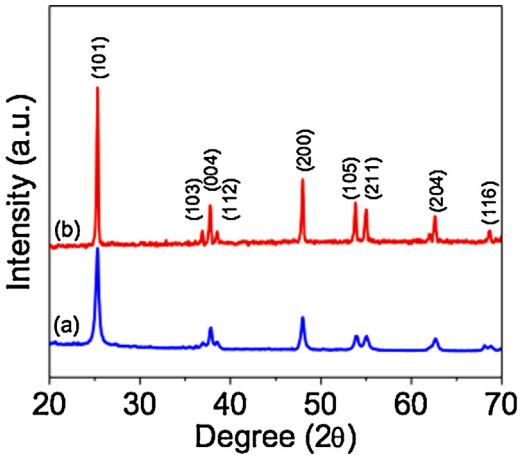

Fig. 2. XRD spectra of (a) NR-NP and (b) NR.

Fig. 3a shows SEM image of the NRs which have average diameter of 50 nm and length of 700 nm. Fig. 3b indicates that the NR-NPs assemblies consist basically of nanoparticles and nanorods which have made surface attachments. TEM images of NR and NR-NP assemblies are given in Figs. 3c and 3d, respectively. The NR-NP assemblies have nanoparticles of ~30 to 60 nm diameter attached to 100 to 600 nm long nanorods. Formation of this kind of structure can be understood on the basis of dissolution-nucleation mechanism proposed by Qiu et al [33]. In the presence of water and DMA, TiO_2 NR precursor dissolves partially into Ti monomer or oligomer and then nucleates as a nanoparticle on the surface of the remained TiO_2 nanorods which eventually take the shape of nanoparticles attached to nanorods assemblies. From energy dispersive spectroscopy (EDS) studies, it was understood that the synthesized layer was highly pure without any contamination (please see the supplementary Fig. S2).

Fig. 4 shows the N_2 adsorption–desorption isotherms obtained from the physisorption measurements. The curves show a combination of types I and IV adsorption–desorption process which is characteristic of microporous and mesoporous substances [34]. Average BET surface area of NRs was 64.6 $m^2 g^{-1}$; while that of NR-NPs was 116.9 $m^2 g^{1}$. The 81% larger surface area of NR-NP was due to the attachment of NPs to the nanorods particles. DSSCs made with NR-NPs provided an extraordinary condition for chemisorption of the dye molecules to the photoelectrodes made. The NR-NPs DSSCs showed a much higher dye adsorption (2.38×10^{-7} mol cm^{-2}) than the NR based DSSCs showing 1.64×10^{-7} mol cm^{-2}.

3.2. Photovoltaic Characteristics

Photocurrent density vs. voltage curves (J–V) of NR and NR-NP DSSCs are compared in Fig. 5a. Corresponding photovoltaic parameters are summarized in Table 1. Nanorod based cell shows current density (J_{sc}) of 14.37 mA/cm^2, open-circuit voltage (V_{oc}) of 0.803 V and fill factor of 0.70. The resulted energy conversion efficiency is 6.29 %.

The energy conversion efficiency is raised to 8.07% when nanorod-nanoparticle assembly is applied as photoanode. This results in a relatively high current density (18.96 mA/cm^2) which directly relates to enhancement of dye loading and the light scattering ability of the photoanode. Since these both parameters significantly influence the light harvesting and thereby the power conversion efficiency, incident photons to current conversion

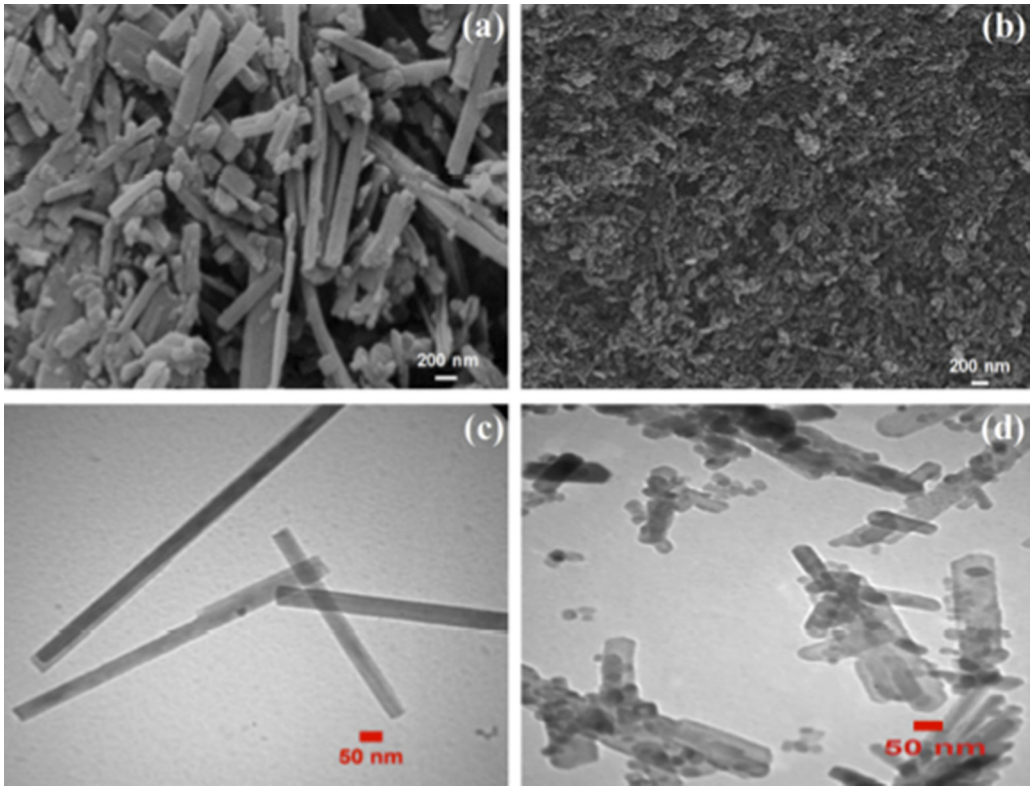

Fig. 3. Scanning Electron Microscopic images of (a) TiO_2 nanorod (NR) and (b) TiO2 nanorod-nanoparticle (NR-NP) and Transmission Electron Microscope images of (c) TiO_2 nanorod (NR) and (d) TiO_2 nanorod-nanoparticle (NR-NP).

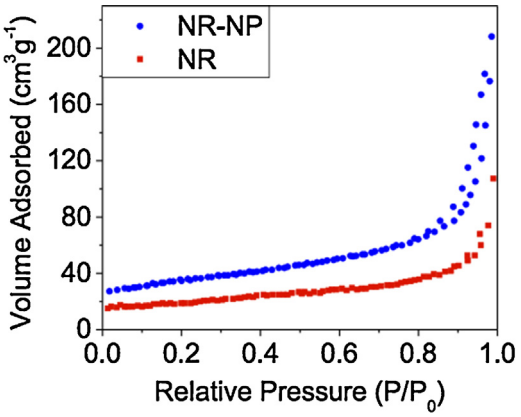

Fig. 4. N_2 adsorption–desorption isotherms measurements of anorod-nanoparticles and nanorods.

efficiency (IPCE) spectra was employed to clarify photovoltaic proficiencies of these DSC cells, as shown in Fig. 5b.

As is observed in Fig. 5b, the external quantum efficiency of NR and NP-NR assembly cells at 530 nm are equal to 78 and 89%, respectively. The high surface area and complex morphology of NP-NR assembly is offering such enhancement in device performance. This structure has high porosity as compared to the nanorods. The N2 adsorption–desorption isotherms confirms these findings. The value of IPCE depends upon different factors include the quantum yield for electron injection from dye in the conduction band of TiO_2 (ϕ_{inj}), charge collection efficiency (η_{coll}) and the light harvesting efficiency for photons of wavelength λ (LHE (λ)) of TiO_2 anode. In section 3.3, EIS analysis will show that η_{coll} of both cells are comparable (52.94% for NR-NP compared with 56.56% for NR) and

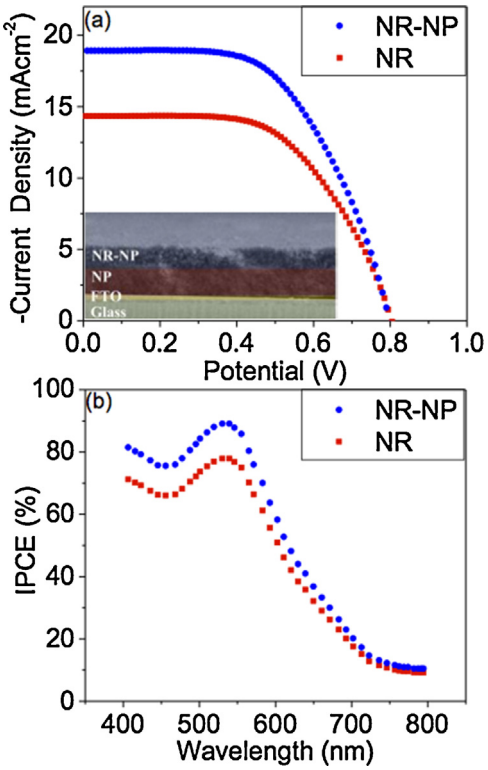

Fig. 5. (a) J–V curves and (b) internal power conversion efficiency (IPCE) spectra of the double layered DSSC cell based on nanorod and nanorod-nanoparticle.

Table 1
Comparison of photovoltaic characteristics of DSSCs made of NR-NP and NP photoanodes.

DSSC device	Surface area ($m^2 g^{-1}$)	Dye absorption (10^{-7} mol cm^{-2})	Voc (V)	Jsc ($mA cm^{-2}$)	FF (%)	Efficiency (%)	IPCE (%)
NR-NP	116.9	2.38	0.795	18.96	0.54	8.07	89.1
NR	64.6	1.64	0.800	14.37	0.58	6.64	77.9

the same dye which has been used for both cells lead to the same ηinj. Consequently, in our research, LHE (λ) is the crucial parameter which governs IPCE. LHE (λ) varies with film thickness (d) and optical absorption cross-section (α) of the sensitizer as described in formulae 1 and 2:[35]

$$\text{LHE}(\lambda) = 1 - 10^{-\alpha d} \quad (1)$$

In which, $\alpha = \sigma c$, (2)

where σ is the sensitizer's concentration in the mesoporous film and c is the velocity of the light. In case of NR-NP anode, the dye loading is higher because of large porosity/surface area which leads to increase the value of σ. The higher value of α will ultimately improve the LHE (λ) in the range of 400–700 nm as per absorption band of dye.

Fig.6 shows the UV–Vis diffuse reflectance spectra of the NR and NR-NP photoanodes with and without dye loading. These spectra were used to evaluate the light scattering abilities of the photoanodes. Apparently, before dye loading (Fig. 6a) the NR-NP retained a higher reflectance than the NR in the whole visible range (400–800 nm), showing that the NR-NP structure reflects the sunlight more efficiently through the photoanode. After dye loading (Fig. 6b), a band in reflectance at around 520 nm for both NR and NR-NP is appeared which is related to the absorbance by the N719 dye in the visible region (Uv–Vis absorbance spectra of

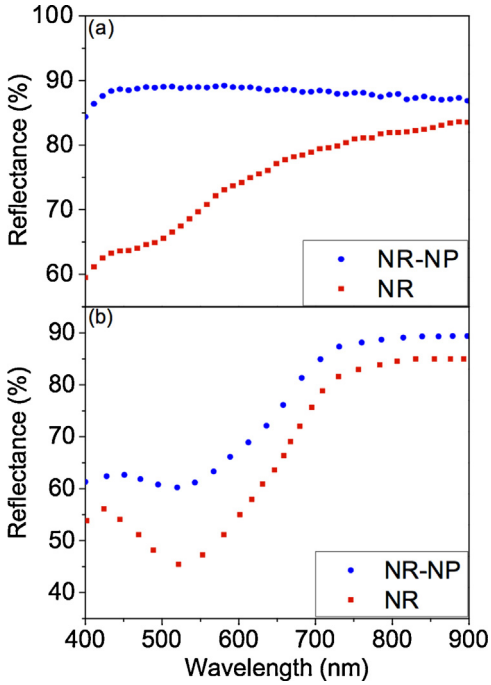

Fig. 6. Diffuse-reflectance spectra of TiO_2 nanorod and nanorod-nanoparticle based photoanode before (a) and after (b) dye loading.

the N719 dye is shown in Fig. S3 as a reference). Moreover, as it can be observed the reflectance of NR-NP decreases drastically from ca. 90% to ca. 60% in the short wavelength (400–600 nm), which is predominantly ascribed to the high light absorption by the dye molecules due to the high surface area. In comparison, the NR depicts a lower decrease in reflectance (from ca. 65% to ca. 45%) at the same wavelength region owing to the low light absorption due to low dye loading. Same as before dye loading, in the whole visible range, the dye-absorbed NR-NP still retained a higher reflectance than the dye absorbed NR. However, it should be mentioned this difference in light scattering efficiency may not be proportional to the difference in IPCE (especially at lambda higher than 700 nm) because number of other parameters can affect IPCE [36].

Consequently, the enhancement in cell performance is related to the excellent management of the light reflection in NR-NP photoanode. As shown in Fig. 1, it can be deduced that, NP-NR assembly significantly creates an obstacle against the incident light (Mie theory [37]) which consequently improves light travelling path in photoanode. Thus, this structural design offers eventually long light diffusion distance through higher chemisorbed dye and results in improvement of the photovoltaic performance of the DSSC.

Though, NR based photoanodes give more proper electron transport paths, however, in case of NP-NR assembly, specific surface morphology provides an optimum condition in order to have higher light scattering and light-dye interaction.

3.3. Transport and recombination properties of photo-generated charge carriers

For further elucidation, electrochemical impedance spectroscopy (EIS) was carried out to study electron recombination and dynamics of the charge transfer processes in the cells. Fig. 7a shows generalized equivalent circuit of the system which corresponds to the transmission line model (supplementary Fig. S4) [38] to fit experimental data of the Nyquist plots (Fig. 7b) under open-circuit conditions and 100 mW/cm^2 solar illumination.

Typically, start point for all of the spectra resemble the R_S which represents the contact impedance between FTO substrate and the metal ohmic contact which is the only real part of the impedance

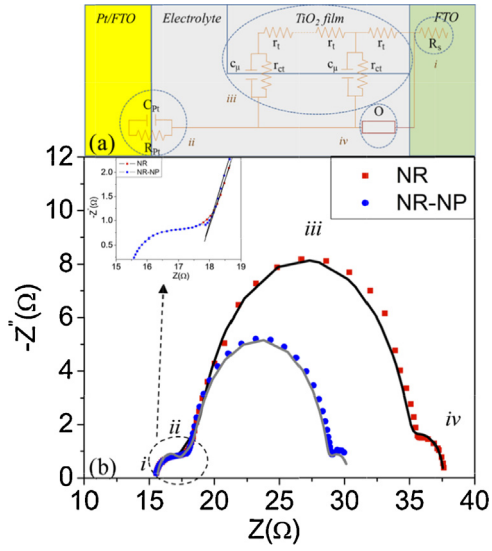

Fig. 7. (a) Generalized equivalent circuit model and (b) Nyquist plots of electrochemical impedance spectroscopy of the DSSCs based on double layered NR, NR-NP photoanodes. (The fitted results are shown with solid line). Inset: straight lines at medium frequencies account for electron transport resistance in the TiO_2 film.

(i). Then, from high to low frequency, the three semicircles in the Nyquist impedance spectra are observed. The small one (ii) in the high frequency region is related to the charge transfer between counter electrode and electrolyte interface (R_{Pt}). The large semicircle (iii) exhibits the charge transfer in the nanocrystalline TiO_2 film (R_t and R_{ct}) and the last one (iv) is related to the electrolyte ion diffusion (O, cotangent hyperbolic which is shown in detail in supplementary Fig. S5) [39].

The simulated data obtained from the equivalent circuit are listed in Table 2, where $r_t = R_t/L$, $r_{ct} = R_{ct}L$ and $c_\mu = C_\mu/L$[22]. The parameters R_t, R_{ct}, C_μ, L and D_e are the electron transport resistance in the TiO_2 film (inset in Fig. 7a: straight line at medium frequencies), interfacial charge transfer resistance because of electron recombination at the TiO_2/electrolyte interface, chemical capacitance caused by the accumulation of electrons in the TiO_2 film, TiO_2 film thickness, and electron diffusion coefficient, respectively [22].

The fitted data show that the R_s and R_{Pt} values for the two DSSCs are the same. This is because of the similarity between the FTO substrate and Pt-counter electrodes. However, NP-NR assembly DSSC exhibits lower R_t and R_{ct} values than that of NR based cell. This indicates that charges can move more straightforwardly from the electrolyte to the dye molecules and from dye molecules into the TiO_2 film in NR-NP based DSSC than the NR DSSC.

The lifetime (τ_e) and transit time (τ_t) of electrons in the TiO_2 film were calculated from formulae 3 and 4:[22]

$$\tau_e = R_{ct} \times C_\mu \quad (3)$$

$$\tau_t = R_t \times C_\mu = L^2/D_e \quad (4)$$

NR and NR-NP cells have electron transit times of 13.17 and 9.62 ms which lead to the electron diffusion of 1.93×10^{-4} cm^2 s^{-1} and 2.64×10^{-4} cm^2 s^{-1} for NR-NP and NR, respectively. Moreover, for the trapping/detrapping dynamics, it is a general rule that a higher electron concentration, *i.e.*, a higher quasi-Fermi level, decreases the transit time, since less energy is needed to transfer electrons from the traps to the conduction band. Consequently, although we should consider the film conductivity, since NR-NP has lower resistance, higher electron diffusion results in higher electron concentration [40] due to the higher light scattering and dye loading behavior. It should be noted that in spite of the higher electron lifetimes (τ_e) of NR cell (30.31 ms versus 20.44 ms for NR-NP) which lead to the slightly higher V_{oc} [13] the charge collection efficiency (η_{coll}, measured from formula 3 [22]) of both cells are comparable (52.94% for NR-NP compared with 56.56% for NR), where: [22]

Table 2
Electron dynamic parameters estimated from the Nyquist impedance plots.

Parameter	NR-NP	NR
R_s (Ω)	15.58	15.56
R_{Pt} (Ω)	1.29	1.02
R_t (Ω)	4.74	6.86
R_{ct} (Ω)	10.07	15.79
C_μ (mF)	2.03	1.92
τ_e (ms)	20.44	30.31
τ_t (ms)	9.62	13.17
D_e ($\times 10^{-4}$ cm^2 s^{-1})	2.64	1.93
η_{coll} (%)	52.94	56.56
L_n (μm)	23.23	24.19
O (Mho)	1.22	0.65
χ^2	0.003	0.169

$$\eta_{coll} = 1 - (\tau_t/\tau_e) \quad (5)$$

Further, J_{sc} can be approximated by the following expression: [22]

$$J_{sc} = I_0 q \eta_{inj} \eta_{coll} \eta_{lh} \quad (6)$$

where I_0 is the light intensity, q is the elementary charge, η_{inj} is the charge injection efficiency (which is in regarded to the dye), η_{coll} is the charge collection efficiency and η_{lh} is the light harvesting efficiency of a cell (which is generally governed by the amount of chemisorbed dye). Since the sensitized dye was the same and also the charge collection efficiency has been perceived to be comparable for both cells, higher light harvesting of the NR-NP cell due to its higher surface area and light scattering ability governs the higher current density [41].

On the other hand, the electron average diffusion length (L_n), which is the average transportation distance of electron before recombination [40], can be calculated by using formula 7:[22]

$$L_n = (D_t \times \tau_e)^{0.5} \quad (7)$$

Diffusion length should meet the criterion $L_n > L$. As listed in Table 2, both cells meet this criterion when having the same value. We also found that the O value of the NR-NP assembly based anode is higher than NR anode (1.22 Mho in comparison to 0.65 Mho). This excellent electrolyte ion, namely I_3^-, diffusion value suggests that the heterostructures of TiO_2 derives a benefit from higher porosity and faster electron path way, as well as good connection with the substrate which permits efficient diffusion of I_3^- ions [39].

All in all, these results confirm that the NR-NP double layer structure with higher levels of dye loading and light harvesting as well as effective electron transport is most favorable to the conversion efficiency of the DSSC. This conclusion is consistent with the I–V performance and IPCE spectra.

4. Conclusions

Hierarchical TiO_2 double layered nanorod-nanoparticle assemblies were successfully synthesized via hydrothermal process. Nanoparticles attached to the nanorods of TiO_2 offered high visible light scattering and dye loading capacity. TiO_2 nanorod-nanoparticles assembly acted as a scatter layer for DSSC photoanode. Consequently, high performance DSSC with efficiency of 8.07%, short circuit current density of 18.96 mA cm^{-2} and open circuit potential of 0.795 V was obtained. The specific surface morphology of TiO_2 heterostructures owed to large surface (116.9 $m^2 g^{-1}$), high dye loading (2.38×10^{-7} mol cm^{-2}) and great light scattering (89.2%) values. In addition, nanoparticles attached to the nanorods showed low charge transfer resistance (10.07 Ω), long electron life time (21.51 ms) and high electrolyte ions diffusion (1.22 Mho) when used in DSSCs.

Acknowledgement

Deputy of research of Sharif University of Technology is thanked for his continued support of research at the frontiers of knowledge.

Appendix A. Supplementary data

Supplementary data associated with this article can be found, in the online version, at http://dx.doi.org/10.1016/j.electacta.2015.04.077.

References

[1] B. O'Regan, M. Grätzel, A low-cost, high-efficiency solar cell based on dye-sensitized colloidal TiO_2 films, Nature 353 (1991) 737.
[2] M. Grätzel, Photoelectrochemical cells, Nature 414 (2001) 338.
[3] M. Hoseinbor, S.K. Sadrnezhaad, S. Daneshvar Asl, Performance Improvement of dye sensitized photovoltaic photocell by using titanium dioxide thin layer doped with lithium, New Processes in Materials Engineering 8 (2014) 1.
[4] K. Guo, M. Li, X. Fang, L. Bai, M. Luoshan, F. Zhang, X. Zhao, Improved properties of dye-sensitized solar cells by multifunctional scattering layer of yolk-shell-like TiO_2 microspheres, J. Power Sources 264 (2014) 35.
[5] K. Zhu, N.R. Neale, A. Miedaner, A.J. Frank, Enhanced Charge-Collection Efficiencies and Light Scattering in Dye-Sensitized Solar Cells Using Oriented TiO_2 Nanotubes Arrays, Nano Lett. 7 (2007) 69.
[6] B.E. Hardin, E.T. Hoke, P.B. Armstrong, J.-H. Yum, P. Comte, T. Torres, J.M.J. Fréchet, M.K. Nazeeruddin, M. Grätzel, M.D. McGehee, Increased light harvesting in dye-sensitized solar cells with energy relay dyes, Nat. Photonics 3 (2009) 406.
[7] Y.-F. Chiang, R.-T. Chen, P.-S. Shen, P. Chen, T.-F. Guo, Extension lifetime for dye-sensitized solar cells through multiple dye adsorption/desorption process, J. Power Sources 225 (2013) 257.
[8] J.Y. Ahn, K.J. Moon, J.H. Kim, S.H. Lee, J.W. Kang, H.W. Lee, S.H. Kim, Designed synthesis and stacking architecture of solid and mesoporous TiO_2 nanoparticles for enhancing the light-harvesting efficiency of dye-sensitized solar cells, ACS Appl. Mater. Interfaces 6 (2014) 903.
[9] K. Fan, W. Zhang, T. Peng, J. Chen, F. Yang, Application of TiO_2 Fusiform Nanorods for Dye-Sensitized Solar Cells with Significantly Improved Efficiency, J. Phys. Chem. C 115 (2011) 17213.
[10] H.-Y. Chen, T.-L. Zhang, J. Fan, D.-B. Kuang, C.-Y. Su, Electrospun hierarchical TiO_2 nanorods with high porosity for efficient dye-sensitized solar cells, ACS Appl. Mater. Interfaces 5 (2013) 9205.
[11] Y. Zhou, X. Wang, H. Wang, Y. Song, L. Fang, N. Ye, L. Wang, Enhanced dye-sensitized solar cells performance using anatase TiO_2 mesocrystals with the Wulff construction of nearly 100% exposed {101} facets as effective light scattering layer, Dalton Trans. 43 (2014) 4711.
[12] C.-S. Chou, M.-G. Guo, K.-H. Liu, Y.-S. Chen, Preparation of TiO_2 particles and their applications in the light scattering layer of a dye-sensitized solar cell, Appl. Energy 92 (2012) 224.
[13] C.-H. Tsai, C.-W. Chang, Y.-T. Tsai, C.-Y. Lu, M.-C. Chen, T.-W. Huang, C.-C. Wu, Novel three-layer TiO_2 nanoparticle stacking architecture for efficient dye-sensitized solar cells, Org. Electron. 14 (2013) 2866.
[14] Y. Qiu, W. Chen, S. Yang, Double-layered photoanodes from variable-size anatase TiO_2 nanospindles: a candidate for high-efficiency dye-sensitized solar cells, Angew. Chem. Int. Ed. Engl. 49 (2010) 3675.
[15] L. Zhu, Y.L. Zhao, X.P. Lin, X.Q. Gu, Y.H. Qiang, The effect of light-scattering layer on the performance of dye-sensitized solar cell assembled using TiO_2 double-layered films as photoanodes, Superlattices Microstruct. 65 (2014) 152.
[16] T.G. Deepak, G.S. Anjusree, S. Thomas, T.a. Arun, S.V. Nair, a. Sreekumaran Nair, A review on materials for light scattering in dye-sensitized solar cells, RSC Adv. 4 (2014) 17615.
[17] L. De Marco, M. Manca, R. Giannuzzi, F. Malara, G. Melcarne, G. Ciccarella, I. Zama, R. Cingolani, G. Gigli, Novel Preparation Method of TiO_2 -Nanorod-Based Photoelectrodes for Dye-Sensitized Solar Cells with Improved Light-Harvesting Efficiency, J. Phys. Chem. C 114 (2010) 4228.
[18] W.-Q. Wu, J.-Y. Liao, H.-Y. Chen, X.-Y. Yu, C.-Y. Su, D.-B. Kuang, Dye-sensitized solar cells based on a double layered TiO_2 photoanode consisting of hierarchical nanowire arrays and nanoparticles with greatly improved photovoltaic performance, J. Mater. Chem. 22 (2012) 18057.
[19] B. Tan, Y. Wu, Dye-Sensitized Solar Cells Based on Anatase TiO_2 Nanoparticle / Nanowire Composites, J. Phys. Chem. B 110 (2006) 15932.
[20] J. Luo, L. Gao, J. Sun, Y. Liu, A bilayer structure of a titania nanoparticle/highly-ordered nanotube array for low-temperature dye-sensitized solar cells, RSC Adv. 2 (2012) 1884.
[21] K.C. Sun, M.B. Qadir, S.H. Jeong, Hydrothermal synthesis of TiO_2 nanotubes and their application as an over-layer for dye-sensitized solar cells, RSC Adv. 4 (2014) 23223.
[22] Y.P. Lin, S.Y. Lin, Y.C. Lee, Y.W. Chen-Yang, High surface area electrospun prickle-like hierarchical anatase TiO_2 nanofibers for dye-sensitized solar cell photoanodes, J. Mater. Chem. A 1 (2013) 9875.
[23] D. Wu, F. Zhu, J. Li, H. Dong, Q. Li, K. Jiang, D. Xu, Monodisperse TiO_2 hierarchical hollow spheres assembled by nanospindles for dye-sensitized solar cells, J. Mater. Chem. 22 (2012) 11665.
[24] J. Jiang, F. Gu, X. Ren, Y. Wang, W. Shao, C. Li, G. Huang, Efficient Light Scattering from One-Pot Solvothermally Derived TiO_2 Nanospindles, Ind. Eng. Chem. Res. 50 (2011) 9003.
[25] U. Opara Krašovec, M. Berginc, M. Hočevar, M. Topič, Unique TiO_2 paste for high efficiency dye-sensitized solar cells, Sol. Energy Mater. Sol. Cells 93 (2009) 379.
[26] S.-Q. Fan, C.-J. Li, G.-J. Yang, L.-Z. Zhang, J.-C. Gao, Y.-X. Xi, Fabrication of Nano-TiO_2 Coating for Dye-Sensitized Solar Cell by Vacuum Cold Spraying at Room Temperature, J. Therm. Spray Technol. 16 (2007) 893.
[27] J. Lin, J. Chen, X. Chen, High-efficiency dye-sensitized solar cells based on robust and both-end-open TiO_2 nanotube membranes, Nanoscale Res. Lett. 6 (2011) 475.
[28] M.Y. Song, D.K. Kim, K.J. Ihn, S.M. Jo, D.Y. Kim, Electrospun TiO_2 electrodes for dye-sensitized solar cells, Nanotechnology 15 (2004) 1861.

[29] S. Ito, P. Chen, P. Comte, M.K. Nazeeruddin, P. Liska, M. Gratzel, Fabrication of Screen-Printing Pastes From TiO_2 Powders for Dye-Sensitised Solar Cells, Prog. Photovoltaics Res. Appl. 15 (2007) 603.
[30] Z.-S. Wang, H. Kawauchi, T. Kashima, H. Arakawa, Significant influence of TiO_2 photoelectrode morphology on the energy conversion efficiency of N719 dye-sensitized solar cell, Coord. Chem. Rev. 248 (2004) 1381.
[31] H.-P. Kuo, C.-F. Yang, A.-N. Huang, C.-T. Wu, W.-C. Pan, Preparation of the working electrode of dye-sensitized solar cells: Effects of screen printing parameters, J. Taiwan Inst. Chem. Eng. 45 (2014) 2340.
[32] M. Montazeri-Pour, N. Riahi-Noori, A. Mehdikhani, Processing Research Synthesis of single-phase anatase TiO_2 nanoparticles by hydrothermal treatment with application potential for photoanode electrodes of dye sensitized solar cells, J. Ceram. Process Res. 14 (2013) 2–7.
[33] Y. Qiu, K. Yan, S. Yang, L. Jin, H. Deng, W. Li, Synthesis of Size-Tunable Anatase TiO_2 Nanospindles and Their Assembly into Anatase@Titanium Oxynitride/Titanium Nitride-Graphene Nanocomposites for Rechargeable Lithium Ion Batteries with High Cycling Performance, ACS Nano 4 (2010) 6515.
[34] J.T. Park, D.K. Roh, R. Patel, E. Kim, D.Y. Ryu, J.H. Kim, Preparation of TiO_2 spheres with hierarchical pores via grafting polymerization and sol–gel process for dye-sensitized solar cells, J. Mater. Chem. 20 (2010) 8521.
[35] M. Gratzel, Solar energy conversion by dye-sensitized photovoltaic cells, Inorg. Chem. 44 (2005) 6841.
[36] P. Cheng, S. Du, Y. Cai, F. Liu, P. Sun, J. Zheng, G. Lu, Tripartite layered photoanode from hierarchical anatase TiO_2 urchin-like spheres and P25: A candidate for enhanced efficiency dye sensitized solar cells, J. Phys. Chem. C 117 (2013) 24150.
[37] A. Hagfeldt, G. Boschloo, L. Sun, L. Kloo, H. Pettersson, Dye-sensitized solar cells, Chem. Rev. 110 (2010) 6595.
[38] J. Bisquert, F. Fabregat-santiago, S. Ferriols, P. Bogdanoff, E.C. Pereira, S.P. Brazil, Doubling Exponent Models for the Analysis of Porous Film Electrodes by Impedance. Relaxation of TiO_2 Nanoporous in Aqueous Solution, J. Phys. Chem. B 104 (2000) 2287.
[39] K. Yan, Y. Qiu, W. Chen, M. Zhang, S. Yang, A double layered photoanode made of highly crystalline TiO_2 nanooctahedra and agglutinated mesoporous TiO_2 microspheres for high efficiency dye sensitized solar cells, Energy Environ. Sci. 4 (2011) 2168.
[40] K. Fredin, Studies of charge transport processes in dye-sensitized solar cells, doctoral thesis, KTH (2007) 17–18.
[41] W.-Q. Wu, Y.-F. Xu, H.-S. Rao, C.-Y. Su, D.-B. Kuang, A double layered TiO_2 photoanode consisting of hierarchical flowers and nanoparticles for high-efficiency dye-sensitized solar cells, Nanoscale 5 (2013) 4362.